CRYSTAL GROWTH & DESIGN

pubs.acs.org/crystal

Article

Using Chemical Substitution to Engineer Photomechanical Cinnamalmalononitrile Crystals

Published as part of Crystal Growth & Design special issue "Honoring Professor Jagadese J. Vittal and his Contributions to Functional Molecular Crystals".

Thomas J. Gately, Cody J. Perry, Sophie Weiss, Kevin Lam, Imadul Islam, Mohammed N. Almtiri, Veronica Carta, Gregory J. O. Beran,* Rabih O. Al-Kaysi,* and Christopher J. Bardeen*

Cite This: *Cryst. Growth Des.* 2024, 24, 9544−9555

Read Online

ACCESS | Metrics & More | Article Recommendations | Supporting Information

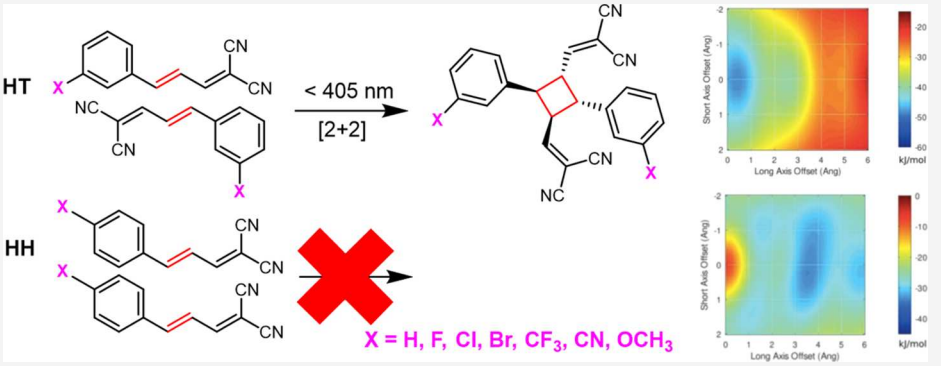

ABSTRACT: In this work, a combined experiment and theory approach is used to study the cinnamalmalononitrile family of molecules that undergo a [2 + 2] photodimerization in the solid-state to generate photomechanical actuation. Twelve new derivatives are synthesized that exhibit two different crystal packing motifs: head-to-head (HH) in which the molecules stack with the phenyl rings on the same side of the stack, and head-to-tail (HT) in which the phenyl rings of adjacent molecules are on opposite sides. [2 + 2] photodimerization is only observed for HT packing motif. Attempts to identify chemical substitution patterns that favor the reactive HT packing based on simple steric and electrostatic considerations fail to reliably predict crystal packing, and fluorination generated both motifs in more-or-less random fashion. Empirically, substitution at the 3-position favors HT packing while substitution at the 4-position favors HH packing. Computational modeling suggests that the tendency for HH or HT packing arrangements stems from complex many-body interactions with the rest of the lattice. Modeling with periodic density functional theory shows that interactions with the rest of the lattice also explain why the HT motif is photochemically active while the HH motif is inert. Chemical substitution can also affect the theoretical photomechanical work output of the HT polymorphs. In order to obtain a reactive HT polymorph, the best strategy appears to entail placing a strong electron-withdrawing group at the 3-position, and we confirm that an HT polymorph of 3-trifluoromethyl- cinnamalmalononitrile is a highly photosalient crystal, with a predicted ideal work density of 40 MJ/m^3.

1. INTRODUCTION

The field of crystal engineering takes a rigorous approach to designing molecules so their crystal packing can generate new physical properties, like solubility, elasticity, and thermal conductivity.[1,2] The ability of the crystal lattice to organize molecules also provides a way to control their reactivity. There are now many examples of how crystal packing can influence reaction outcomes, starting with the seminal work of Schmidt and co-workers that gave rise to the concept of top-ochemistry.[3−5] Much of that foundational work concerned [2 + 2] photocycloaddition reactions between cinnamate derivatives, and this reaction has continued to be a workhorse of the field.[6] Its synthetic utility has been demonstrated by the work of MacGillivray and others, and it has been used to create highly crystalline polymer solids as well.[7,8] This solid-state reaction has also been harnessed to generate photomechanical motion.[9−17] Vittal and co-workers pioneered a supramolecular

Received: July 24, 2024
Revised: October 26, 2024
Accepted: October 28, 2024
Published: November 11, 2024

Scheme 1. (a) Adding Substituents at the 4-Position can Lead to Steric Interference When Adopting HH Packing (Left) while the 3-Position can Largely Avoid the Steric Interference in HH Stacking (Right). (b) For Molecules with a Large Dipole Difference between Ends of the Molecule HT Packing Maximizes the Coulomb Interaction (Left) while a Molecule with a Small Dipole has Less of a Difference between HH and HT Packing

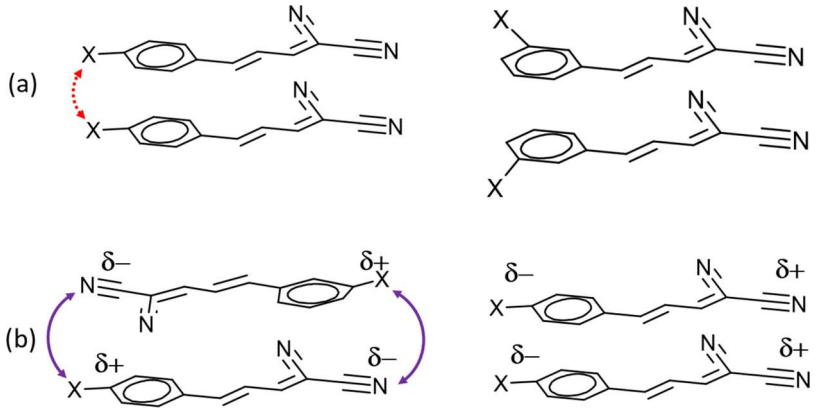

approach that resulted in crystals that exhibit dramatic photosalient effects,[18−23] a general phenomenon in which the photochemical creation of the product raises the potential energy inside the crystal until it is suddenly released as kinetic energy by a combination of fracture and/or phase change.[24,25] Although the [2 + 2] photodimerization is not easily reversed, it provides a useful way to investigate how molecular-level reactions can combine to generate a macroscopic mechanical effect.

We became interested in the potential of the [2 + 2] photocycloaddition reaction for force generation after observing that the bimolecular reaction of crystalline 4-fluorocinnamate (**4FCM**) could produce ∼10× more work in a bending ceramic template that the diarylethene derivatives used previously.[26] This class of molecules utilizes a divinyl side group to increase conjugation and shift the absorption to longer wavelengths and had previously been shown to be photochemically active in crystal form.[27] We sought to improve the performance of this molecule by adding fluorine atoms to the phenyl ring and found that the derivatives all crystallized into one of two characteristic packing motifs.[28] In the head-to-head (HH) motif, the molecules stack with the phenyl rings on the same side of the stack, while in the head-to-tail (HT) motif the phenyl rings of adjacent molecules are on opposite sides. As long as the reactive double bonds are within 4.2 Å of each other, the HT packing motif supports rapid [2 + 2] photodimerization, while the HH motif is unreactive regardless of the double bond separation. Because of the different HH versus HT reactivities, the crystal packing controls the ability of **cinnamalmalononitrile (CM)** derivatives to function as photomechanical materials. Computational work indicated that the HH and HT polymorph energies were often within 1−3 kJ/mol of each other. In some cases, the same molecule could be crystallized in either polymorph by changing the growth solvent.[28]

The complex crystallization behavior of the **CM** derivatives, combined with their potential utility as photomechanical materials, motivated us to study them in greater detail. In particular, we wanted to understand what factors control HH versus HT crystal packing, since this determines whether the crystal can be photomechanically active. Our goal was to test two simple hypotheses. First, we reasoned that substituents at the 4-position will increase steric repulsion for molecules stacked in the HH geometry, raising its energy. On the other hand, substituents at the 3-position can align on opposite sides of the stack in the HH motif and avoid this steric interference. These effects are illustrated in Scheme 1a. The steric interference hypothesis predicts that substitution at the 4-position will favor HT packing, while substitution at the 3-position will produce more HH crystals. The second hypothesis centers on electrostatic interactions between neighboring molecules. The addition or removal of electron density from the phenyl ring should affect its interaction with the electronegative CN groups of neighboring molecules. If the molecule is thought of as a large dipole, then a larger dipole moment should favor HT packing to maximize the Coulomb stabilization. On the other hand, substituents that decrease the net dipole should reduce the Coulomb interaction and make the HH geometry more likely to be observed. This effect is illustrated in Scheme 1b. If validated, these two hypotheses could provide a framework for the design of new materials based on the **CM** framework.

In this paper, we show experimentally that the reasoning described above, based on simple steric and electrostatic considerations of the monomer pair, fails to reliably predict the crystal structure trends observed for the 23 molecules reported here and in our previous paper.[28] In fact, we find that most derivatives behave opposite to the expected trends, with substitution at the 3-position being the most likely to yield the reactive HT form. To better understand these experimental results, we turn to computational modeling. Calculations show that there is a competition between the interactions within the monomer pair, which favor HT packing, and those between the pair and the rest of the lattice that favor the HH motif. By modeling the solid-state transformations with periodic density functional theory (DFT), we find that this competition between the interactions within the monomer pair and those of the pair with the rest of the lattice is also fundamentally related to the experimentally observed differences in the HH and HT solid-state reactivities. Finally, chemical substitution not only controls crystal packing and reactivity but can also affect the photomechanical work output, with a significant variation in work between HT polymorphs composed of different molecules. The results in this paper significantly expand the available library of photoreactive phenyl-divinyl molecules and their crystal structures, providing a new testbed

https://doi.org/10.1021/acs.cgd.4c01033
Cryst. Growth Des. 2024, 24, 9544−9555

Table 1. New CM Derivatives Examined in this Paper and the Abbreviations Used

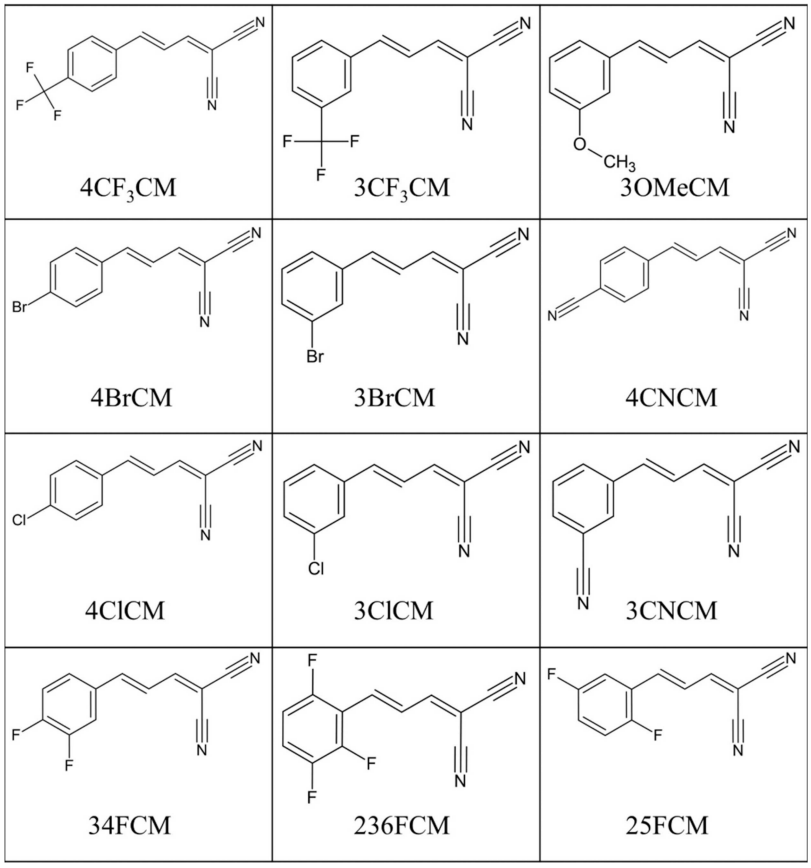

for theoretical crystal structure prediction models. Eventually, these models will guide the development of new design principles for improved photoresponsive molecular crystals.

2. EXPERIMENTAL AND COMPUTATIONAL METHODS

2.1. Sample Preparation. The detailed synthesis of previously unreported **CM** derivatives can be found in the Supporting Information. Most crystals were grown by solvent evaporation. Typically, 4 mg of the compound was dissolved in 2 mL of solvent. For all compounds, crystallization was attempted in both a protic solvent (methanol or ethanol) and an aprotic solvent ($CHCl_3$ or toluene). Testing different solvents was necessary because we previously found that different solvents could generate different polymorphs.[28] The solutions were placed, in a loosely capped vial and stored in a dark cabinet while the solvent was allowed to evaporate over several days. Some growth solutions were placed in the refrigerator to slow the evaporation rate and enhance crystal quality. **3CNCM** and the **4ClCM** crystals were grown using the solvent diffusion method. The compound was dissolved in chloroform in a 5 mL vial that was then placed open in a 20 mL jar containing isopropyl alcohol. As the alcohol diffused into the $CHCl_3$, the crystals grew over the course of a several days. All samples were protected from light exposure during growth.

2.2. Sample Characterization. Crystal structures were obtained using a Bruker D8 Venture Duo diffractometer. Details of the X-ray diffraction analysis for each molecule can be found in the Supporting Information. For microscopic observation of the crystals, an Olympus IX70-inverted microscope with an IX-FLA fluorescence observation attachment with 365, 405, 465, and 532 nm filter cubes was used. Images and videos were obtained using an Amscope MU1000 camera. For solution-state spectroscopic measurements, samples were prepared by dissolving approximately 1 mg of compound in 10 mL of chloroform. The solution was then placed into a quartz cuvette with a 1 cm path length and analyzed in a Cary 60 spectrometer from 200 to 800 nm using a scan speed of 600 nm/min.

2.3. Computational Methods. *2.3.1. Gas-Phase Monomer Studies.* For isolated molecules, dipole moments were calculated using Gaussian 16 software. The structures were optimized using the B3LYP functional and cc-pVDZ basis set.

2.3.2. Gas-Phase Monomer Pair Studies. Initial gas-phase studies of HH and HT monomer pairs were carried out using zeroth-order symmetry adapted perturbation theory (SAPT0),[29,30] which naturally decomposes intermolecular interaction energies into contributions arising from short-range exchange-repulsion, electrostatics, induction, and dispersion. The calculations employed PSI4 v1.7[31] and the jun-cc-pVDZ basis, which performed well in an earlier benchmark study.[32] After optimizing the monomer molecular structures with r^2SCAN-3c,[33] π-stacked monomer pairs were created with a 3.5 Å intermolecular separation. Two-dimensional interaction surfaces were then computed by displacing one rigid monomer relative to the other along the long and short axes of the molecule (holding the 3.5 Å separation constant).

2.3.3. Solid-State DFT. To model the solid-state systems, the experimental crystal structures were optimized in Quantum Espresso 6.5[34] under periodic boundary conditions using the B86bPBE density functional[35,36] with the exchange hole dipole moment (XDM) dispersion correction.[37] A 50 Ry plane-wave cutoff was combined with the projector augmented wave (PAW) treatment of core electrons. A Monkhorst-Pack reciprocal space k-point grid spacing of at least 0.05 $Å^{-1}$ was used.

Generalized gradient approximate (GGA) density functionals such as B86bPBE are convenient for solid-state electronic structure calculations due to their relatively low computational cost, but they suffer from density-driven delocalization error,[38] which can lead to artificial stabilization of species exhibiting greater electron delocalization relative to those that do not.[39] The [2 + 2]-photodimerization

https://doi.org/10.1021/acs.cgd.4c01033
Cryst. Growth Des. 2024, 24, 9544−9555

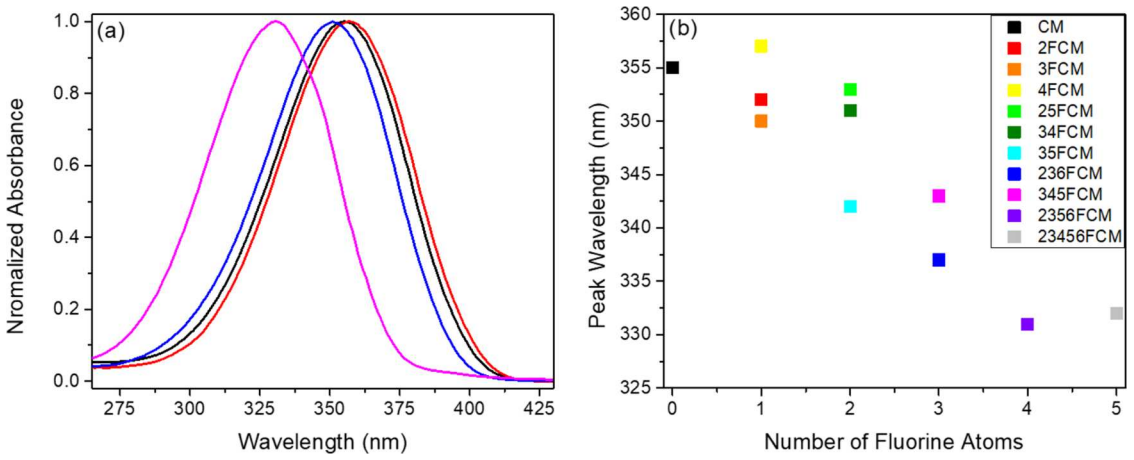

Figure 1. (a) The absorption changes of a single fluorine substitution at various positions on **CM**. Black shows the spectra of unsubstituted **CM**, red shows **4FCM**, blue shows **34FCM**, and purple represents **2356FCM**. (b) The shift in absorption from adding additional fluorine atoms to the **CM** structure.

disrupts the π-conjugation in the **CM** species, resulting in a more localized electron density in the product molecule than in the reactants. As a result, delocalization error in a GGA functional will spuriously destabilize the photodimer product species relative to the reactants.[40] To address delocalization error in the GGA functional used in this work and obtain more realistic energetics, a single-point intramolecular energy correction is applied to the final optimized crystal energies using a higher level of theory[41]—in this case, the double-hybrid revDSD-PBEP86 functional and D4 dispersion correction.[42] In this approach, one computes the periodic B86bPBE-XDM energy of the crystal, subtracts out the gas-phase B86bPBE-XDM energy of each isolated molecule in the unit cell (retaining the crystalline geometry), and adds the gas-phase revDSD-PBEP86-D4 ("Higher") energy of each isolated molecule

$$E_{\text{crystal}}^{\text{corrected}} = E_{\text{crystal}}^{\text{GGA}} + \sum_{i} (E_{\text{molec},i}^{\text{Higher}} - E_{\text{molec},i}^{\text{GGA}}) \quad (1)$$

This approximation amounts to computing the intramolecular interactions with revDSD-PBEP86-D4, and the intermolecular interactions with the lattice with B86bPBE-XDM. The gas-phase B86bPBE-XDM energies are calculated in Quantum Espresso using the same settings, except the molecules are placed in a large periodic box with at least 20 Å spacing in all directions to minimize the interactions between the molecule in its periodic images. See ref 41 for details. The revDSD-PBEP86-D4 energies were calculated in Orca 5.0[43] in the def2-QZVP basis set. In practice, the intramolecular corrections only needs to be computed for each symmetrically unique molecule in the unit cell, and the results can be multiplied by the number of equivalent molecules in the unit cell.

2.3.4. Modeling the Solid-State Photomechanical Responses. Techniques developed in ref 44 were employed to study the [2 + 2] photochemical reactivity and resulting photomechanical responses of the crystals. In brief, this idealized model assumes the photochemical reaction occurs instantly and completely, resulting in a "proto-SSRD" crystal structure which contains the photodimer product molecules within the unit cell of the reactant crystal. Starting from the DFT-optimized monomer crystal structure, the proto-SSRD is generated by replacing pairs of topochemically reacting monomers in the crystal with the photodimer product and minimizing the orientational and translational displacement. A fixed-lattice parameter DFT optimization of this structure that produces the final proto-SSRD. Next, a variable unit cell DFT optimization is performed to relax the proto-SSRD to the equilibrium SSRD crystal structure. This process deforms the crystal, and the associated the anisotropic work density can be computed from the stress and strain associated with the proto-SSRD relative to the equilibrium SSRD. The idealized photomechanical approach provides an upper-bound estimate for the amount of work that could be performed, since experimental photomechanical crystals may not react to 100% completion, and they will likely react more slowly and generate less stress by allowing the lattice to relax as the molecules react. This topochemical modeling approach has correctly predicted the product crystal structures that result from the solid-state photochemical reactions of anthracenes and diarylethenes.[44,45]

3. EXPERIMENTAL RESULTS

Our synthetic strategy for making the various **CM** derivatives is modular and provides a way to rapidly generate a library of different compounds. Details of the synthesis and characterization the 12 new **CM** derivatives (structures shown in Table 1) are given in the Supporting Information. This set of molecules significantly expands the library of **CM** molecules beyond the 11 derivatives described in our first paper.[28] This new set of molecules has two purposes. First, we wanted to expand the library of fluorinated derivatives to fill in some gaps in our previous paper. The molecules **25FCM**, **34FCM**, and **236FCM** provide new molecules to test whether increasing the electron withdrawing power attached to the phenyl can favor the HT motif. The other 9 molecules were prepared in order to examine whether substituents (X) at the 3-position (denoted **3XCM**) and the 4-position (denoted **4XCM**) can favor HT versus HH packing. Including results from our previous paper, the 3 and 4-position substituents are (from smallest to largest): H, F, Cl, Br, CN, CF_3, and OCH_3. This series of substituents was chosen because (a) they provided a large range of sizes and electron withdrawing/donating character; and (b) they provided crystals suitable for X-ray structure determination. We synthesized **CM** molecules with other substituent groups, but if crystals suitable for X-ray structure determination could not be grown, they were not included in this study. For example, several CH_3 derivatives were synthesized, but they had surprisingly low solubility and we could not obtain crystals suitable for X-ray diffraction (XRD) structure determination.

The ability of different substituents to modify the electronic structure of the conjugated **CM** core could be inferred from changes in the electronic absorption spectra. The strong electron-withdrawing CN groups, combined with the extended conjugation of the divinyl tail, impart some charge-transfer (CT) character to the absorption spectrum, which helps shift the absorption peak of **CM** to ~350 nm as compared to a cinnamate whose absorption spectrum typically peaks around 300 nm. But this CT character can be partially canceled out by placing fluorine atoms on the phenyl ring. Figure 1a shows how the addition of F atoms systematically shifts the absorption peak relative to **CM**, without any appreciable change in the absorption line shape. When all the fluorinated compounds were analyzed together, we

https://doi.org/10.1021/acs.cgd.4c01033
Cryst. Growth Des. 2024, 24, 9544−9555

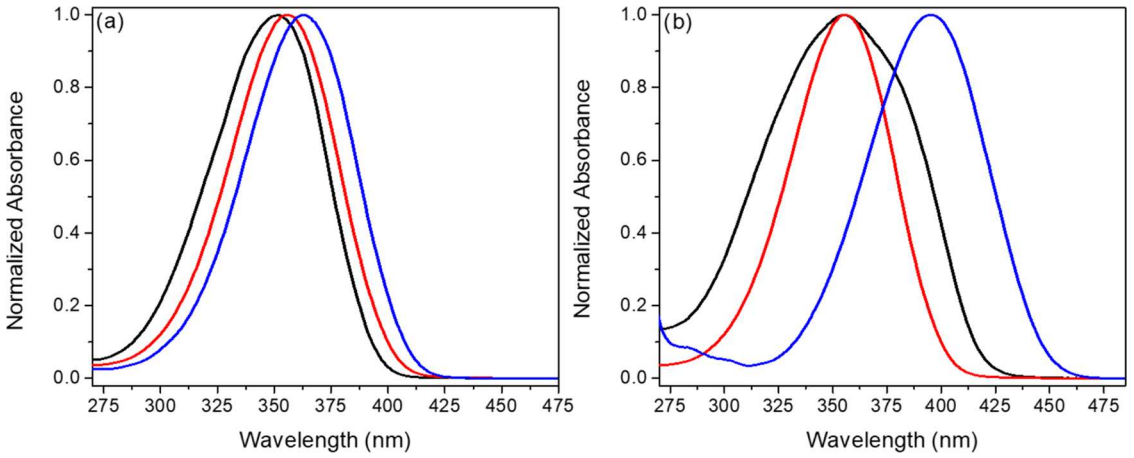

Figure 2. Shift in absorbance of the **3XCMs** and **4XCMs** with different substituents. Panel (a) shows **CM** (red) with a λ_{max} of 356 nm, **3BrCM** (black) with a λ_{max} of 352 nm and **4BrCM** (blue) with a λ_{max} of 363 nm. Panel (b) shows unsubstituted **CM** (red) **3MethoxyCM** (black) with a λ_{max} of 355 nm and **4MethoxyCM** (blue) with a λ_{max} of 395 nm.

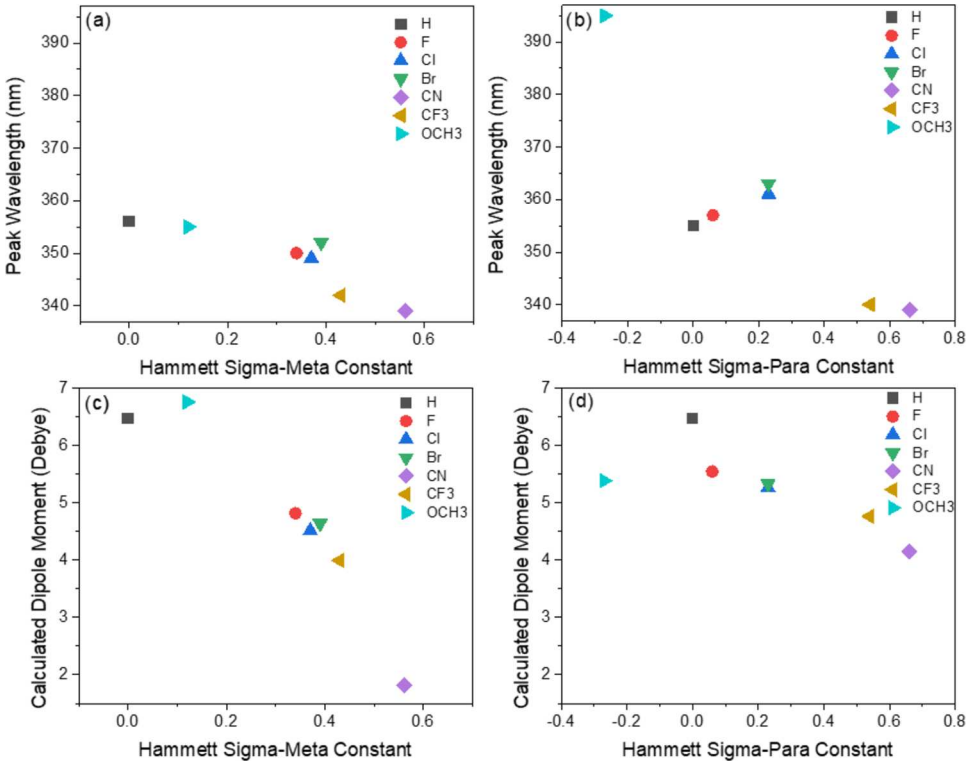

Figure 3. Peak wavelength absorption plotted against the Hammett sigma parameter for (a) the meta substituted **3XCMs** and (b) the para substituted **4XCMs**. The calculated molecular dipole moment plotted against the Hammett sigma parameter for (c) the meta substituted **3XCMs** and (d) the para substituted **4XCMs**.

found that increasing the number of F atoms systematically shifted the absorption peak to higher energies, as seen from the plot in Figure 1b.

Substitution of other chemical groups at the 3- and 4-positions can also lead to substantial changes in the absorption spectrum. We find that substitution at the 4-position has a much larger effect on the absorption than at the 3-position. Since a group at the 4-position is *para* to the divinyl tail, it will be conjugated with this group and is expected to have a larger effect than a substituent at the *meta* position. This is consistent with the smaller absorption peak shifts seen for the **3XCMs** when compared to the **4XCMs**, as illustrated for X = Br (Figure 2a) and X = OCH_3 (Figure 2b). In order to quantify the character of different phenyl ring substituents, we elected to use the Hammett sigma parameter, which has shown to correlate with both electronic absorption peak shifts[46−48] and molecular dipole moments[49,50] of aromatic systems. In both the **3XCMs** and **4XCMs**, we found a good correlation between the peak absorption energy and the Hammett sigma parameter, as shown in Figure 3a,b. The calculated molecular dipole moment was also correlated with this parameter, as shown in Figure 3c,d. Together, these plots confirm that the various substituents have a systematic effect on the electron density distribution in the molecule. The next question is whether these changes influence the crystal packing in a systematic way.

When crystallized, we were surprised to find that all the new fluorinated **CMs** packed in the nonreactive HH motif. This observation showed that F substitution does not systematically favor one packing motif over the other. Symmetric fluorine substitution in the molecules **4FCM** (HH/HT), **25FCM** (HH), **345FCM** (HH), **2356FCM** (HH) and **23456FCM** (HH/HT)

https://doi.org/10.1021/acs.cgd.4c01033
Cryst. Growth Des. 2024, 24, 9544−9555

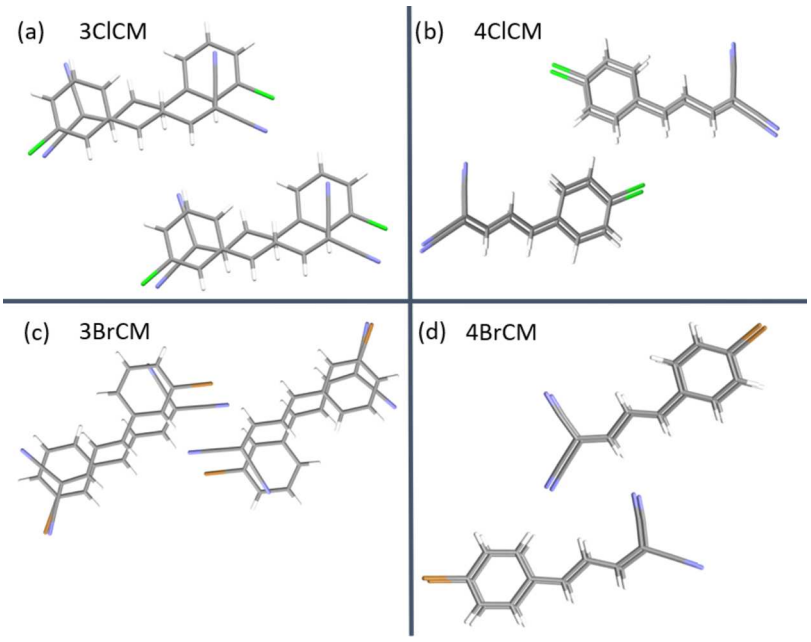

Figure 4. (a) for **3ClCM** HT packing while (b) **4ClCM** shows HH packing. (b) The same trend is seen in (c) **3BrCM** and (d) **4BrCM**.

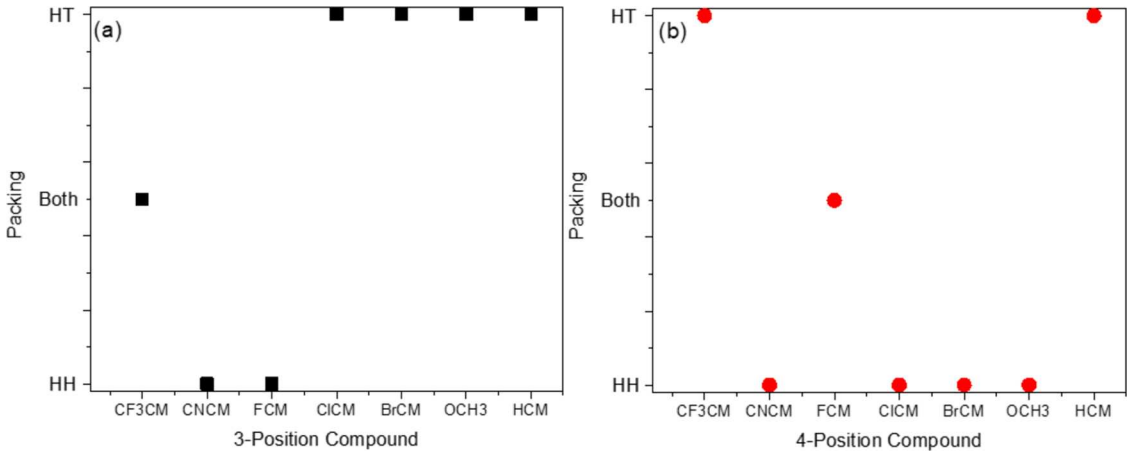

Figure 5. (a) The packing trends for the **3XCMs** favoring HT packing. (b) the packing trends for the **4XCMs** favoring HH packing.

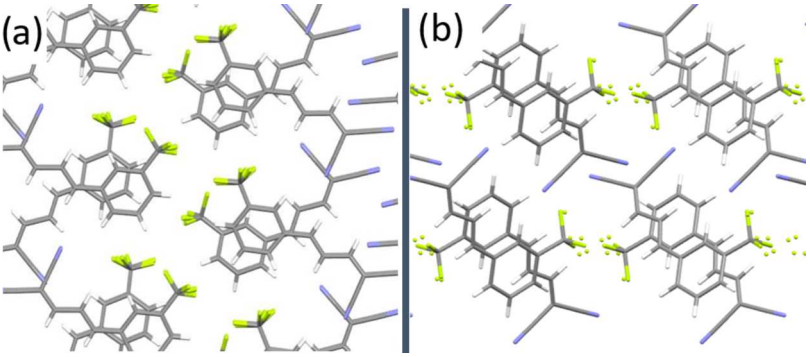

Figure 6. (a) **3CF$_3$CM** gives rise to the expected HH packing which is offset by approximately 45°. (b) **3CF$_3$CM** showing the HT packing motif.

yielded the HH and HT forms with roughly equal probability. Asymmetric substitution in the molecules **2FCM** (HT), **3FCM** (HH), **24FCM** (HT), **34FCM** (HH), and **236FCM** (HH) also yielded a similar number of HH and HT forms. No obvious pattern could be extracted from the results. Previous theory suggested that the HH and HT forms were very close in energy,[28] and indeed both polymorphs could be grown from **4FCM** and **23456FCM**. It is possible that all the fluorinated derivatives possess HH and HT polymorphs that could be uncovered by an exhaustive search of the crystal growth conditions. However, from our results it is clear that although F atoms are known to be effective crystal growth directors, in the **CMs** they cannot steer the packing toward either HH or HT motifs in a systematic way.

https://doi.org/10.1021/acs.cgd.4c01033
Cryst. Growth Des. 2024, 24, 9544−9555

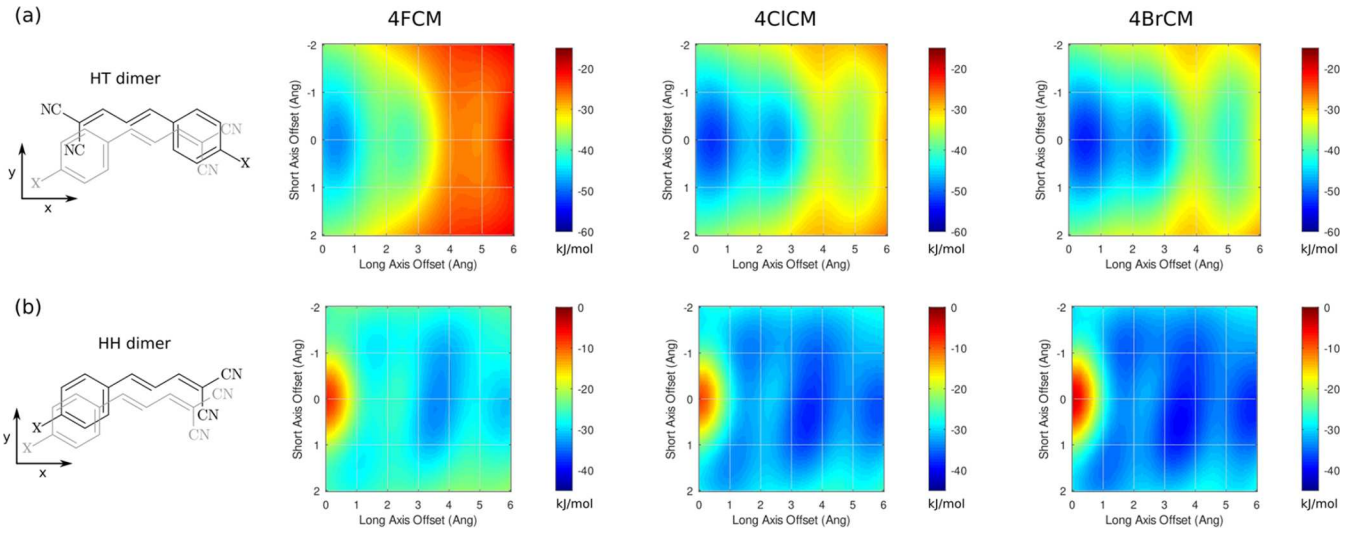

Figure 7. Rigid-molecule SAPT0/jun-cc-pVDZ potential energy scans (kJ/mol) showing how substituting increasingly large halogens in the 4-position impacts the intermolecular interactions. Note that the (a) HT and (b) HH energy scales differ to enable clear visualization of the local minima.

When the phenyl ring substitution position was fixed and the chemical nature of the substituent was varied, we began to see patterns emerge. Substitution at the 3-position produced crystals that were mostly of the HT form, while substitution at the 4-position favored the HH form. Examples of this effect are shown in Figure 4a,b for **3ClCM** versus **4ClCM**, and for **3BrCM** versus **4BrCM** in Figure 4c,d. The complete trend for the **3XCMs** is shown in Figure 5a, where the presence of both HH and HT polymorphs is represented as an intermediate point between the HH and HT extremes. Except for **3CNCM** and **3FCM**, all molecules with a substituent at the 3-position support an HT crystal form. Figure 5b shows the HH/HT trend for the **4XCMs**, where the majority exhibit HH packing.

The different crystal packings gave rise to the expected differences in photomechanical behavior. All the HT crystals exhibited rapid photoreaction and a photosalient response except for **4CF$_3$CM**, which packs in an offset HT geometry with the double bonds separated by 4.3 Å, just outside the range for photodimerization.[51] Examples of photomechanical response for some of the HH **3XCM** crystals (**3CF$_3$CM**, **3ClCM**, **3BrCM**) are shown in the Supporting Information, Videos S1−S3. In contrast, all HH crystals were highly fluorescent and showed almost no motion under illumination. Examples of this lack of response for **4BrCM** and **4ClCM** are shown in the Supporting Information, Videos S4−S5. After extended exposure to ultraviolet light (10 min or more), they sometimes exhibited fading and slight bending, but we attributed this to heating and/or reaction at induced defect sites, rather than to intrinsic reactivity. It is noteworthy that crystallization of **3CF$_3$CM** from a nonpolar solvent like xylene causes it to grow in a modified HH motif with the molecules twisted at ∼45° with respect to each other, as shown in Figure 6a. This twisted form may be an indication that the bulky CF_3 groups interfere with the $\pi-\pi$ interactions that would be expected to drive HH stacking. This polymorph appears to be photochemically inactive due to a misalignment of the double bonds, despite the fact that they are relatively close (3.64 Å). The HT form was obtained by crystallization from a polar solvent like $CHCl_3$, and it reacted rapidly and violently when exposed to ultraviolet light. In our experience, the photosalient effect can be strongly attenuated when the crystals are submerged in a viscous medium, but **3CF$_3$CM** showed strong photosalient behavior even when submerged in highly viscous glycerol. Examples of this response are shown in videos in the Supporting Information, Video S6. It had a much larger photosalient response than the other crystals studied in this work.

4. DISCUSSION AND COMPUTATIONAL ANALYSIS

4.1. Origins of HH versus HT Packing. The results in Figure 5 provide strong evidence that our original steric hypothesis was not correct. We hypothesized that substituents at the 4-position of the phenyl ring would interfere with each other, and this should favor the HT form so the two neighboring groups could avoid interacting with each other. Meanwhile, the ability of the **3XCMs** to stack in the HH form with the substituents on alternating sides would lower the energy of this motif and make it more commonly observed. Instead, we found the opposite trend: **3XCMs** favor HT packing, while **4XCMs** favor HH packing. For the **3XCMs** that did exhibit HH packing (X = CN, F), the X groups line up on the same side in the crystal stacks, with no evidence for the alternating side-group stacking that we hypothesized at the beginning of this work. The data in Figure 5b show that putting bulky groups at the 4-position is not a viable strategy to enforce HT packing.

If we consider simple electrostatic effects, it is again difficult to rationalize the trends shown in Figure 5. For the **3XCMs**, the two molecules that support the HH form, **3CNCM** and **3FCM**, have very different dipole moments, while the molecules with intermediate dipole moments support HT packing. Only **3CNCM** has an anomalously low dipole moment (1.8 D) that would be expected to favor HH packing. Substituents at the 4-position are expected to have a much larger effect on the molecular electron density because they are para to the divinyl tail. But here again there is no clear pattern, with HT packing observed for both large dipoles (**CM**) and much smaller dipoles (**3CF$_3$CM**), while intermediate dipoles exhibit HH packing. It appears that coarse measures of electron density, like the molecular dipole moment, are not sufficient to predict crystal structure trends in the **CM** class of molecules.

The failure of our crystal packing predictions based on simplistic two-body molecular interactions points to the need for a more sophisticated theoretical approach that can handle many-body interactions. In fact, when molecular pairs are considered by themselves, the HT packing is always favored. Gas-phase symmetry-adapted perturbation theory (SAPT0)

https://doi.org/10.1021/acs.cgd.4c01033
Cryst. Growth Des. 2024, 24, 9544−9555

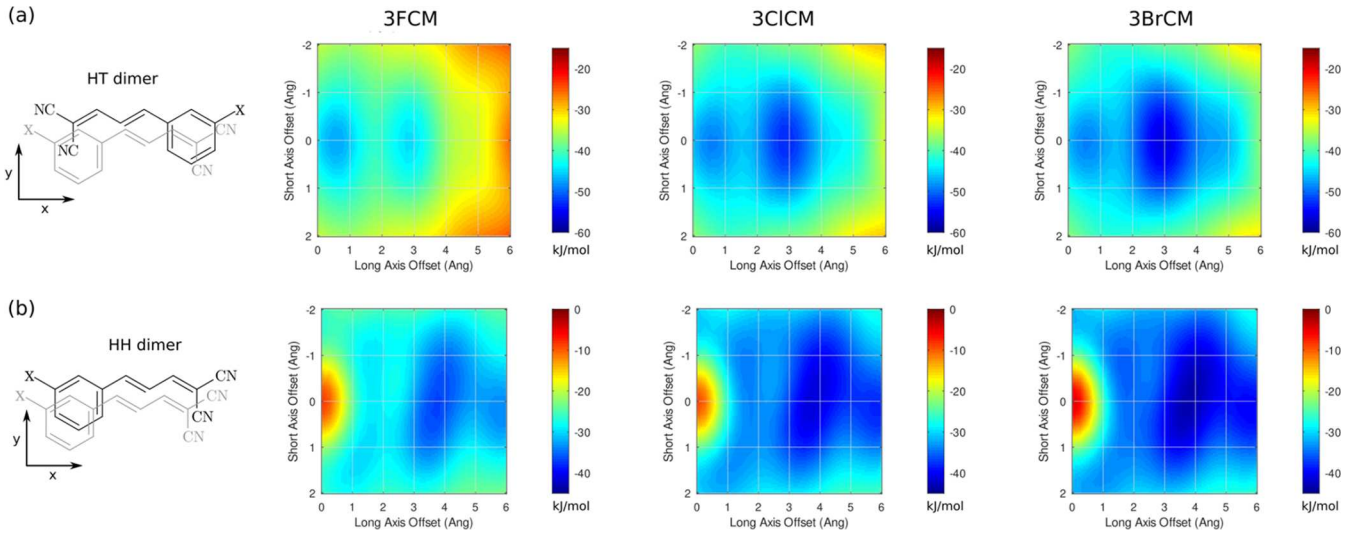

Figure 8. Rigid-molecule SAPT0/jun-cc-pVDZ potential energy scans (kJ/mol) showing how substituting increasingly large halogens in the 3-position impacts the intermolecular interactions. Note that the (a) HT and (b) HH energy scales differ to enable clear visualization of the local minima.

calculations on π-stacked HH and HT monomer pairs of **3XCM**, and **4XCM** (X = F, Cl, or Br) and a 3.5 Å separation between the molecules indicate that the HT pair stacks arrangements bind ∼10−20 kJ/mol more strongly than the HH ones (Figures 7 and 8). For hydrogen and smaller halogens, the optimal HT stacking arrangement involves one molecule being slightly displaced (typically by ∼1 Å) along the long (x) axis relative to the other, though the energetic penalty for small (<1 Å) lateral displacements along the short (y) axis is modest. As the halogen grows in size, however, larger displacements along both axes become increasingly favorable. The preferred HH stacking geometry involves either a large, ∼3−3.5 Å displacement along the long axis or simultaneous ∼1−1.5 Å displacements along both the long (x) and short (y) axes of the molecule. The local minima observed in these monomer pair scans, particularly those with more modest displacements, are generally consistent with the arrangements observed in the experimental crystal structures. Comparing Figures 7 and 8, one also sees that the **3XCM** monomer pairs frequently bind more strongly than the **4XCM** pairs, though the differences are fairly similar across both HH and HT arrangements. The SAPT0 energy decomposition (Figures S41−S46) reveals that HT stacked monomer pairs benefit from stronger electrostatic attractions and reduced short-range exchange-repulsion interactions (i.e., less steric interference) while the HH interactions exhibit moderately stronger attractive van der Waals dispersion interactions. The attractive induction (polarization) contributions are similar across both HH and HT monomer pairs.

Unfortunately, isolated pair interaction energies do not provide a clear rationale for why certain derivatives adopt HT or HH packing motifs in the solid state. Given that the HH stacks consistently exhibit weaker pairwise interactions than HT ones, the HH crystals must compensate by forming stronger many-body interactions with the rest of the lattice such that they achieve similar total lattice energies. For example, **4FCM**, **3ClCM**, and **3CF$_3$CM** exhibit two polymorphs each with different dimer arrangements that differ by only ∼1 kJ/mol in lattice energy according to periodic B86bPBE-XDM DFT calculations. The calculations suggest that the nonreactive HH polymorph of **4FCM**, the reactive colorless polymorph of **3ClCM**, and the reactive HT polymorph of **3CF$_3$CM** are the more stable polymorphs by 1.3, 1.0, and 1.3 kJ/mol, respectively (though such small lattice energy differences could easily be reversed by errors in the DFT models and/or finite-temperature free energy contributions). Additional evidence for the energy compensation between HH and HT motifs in the solid-state comes from our earlier crystal structure prediction study which found many found many energetically competitive HH and HT structures for both for **CM** and **4FCM**.[28]

Finally, we partition the lattice energies for 10 experimental crystals into the contributions stemming from the interaction of the HH or HT monomer pair and from the interactions of that pair with the rest of the lattice. This set includes five HT crystals (**CM**, **4FCM**, **3ClCM**, **3CF$_3$CM**, and **24FCM**) and five HH ones (**3FCM**, **4FCM**, **25FCM**, **26FCM**, and **4CNCM**). In the absence of the surrounding lattice, the 21 kJ/mol average HT monomer pair interaction energy component of the lattice energy is 9 kJ/mol stronger than the 12 kJ/mol average HH interaction. On the other hand, the HH crystals compensate for these weaker interactions within the noncovalent monomer pair through interactions with the rest of the lattice that are 12 kJ/mol stronger than for the HT ones on average.

In summary, it is difficult to assess whether a HH or HT crystal will form based on the monomer pair alone; rather, it is driven by a competition between the interactions within the monomer pair and the interactions of that pair with the rest of the lattice. Identifying specific, universal lattice interactions that stabilize the HH crystals is difficult, due to the wide variety of the crystal packing motifs. From the dense crystal energy landscapes found for **CM** and **4FCM** in the earlier crystal structure prediction study[28] and the two additional examples of experimental polymorphs discussed here, it seems likely that polymorphism is probably thermodynamically feasible for many of these systems. Whether those polymorphs are observed experimentally may simply be a matter of the crystallization kinetics and conditions.

https://doi.org/10.1021/acs.cgd.4c01033
Cryst. Growth Des. 2024, 24, 9544−9555

4.2. Reactivity Differences between HH and HT Crystals. To understand why the HT crystals react while the HH ones do not, we modeled the solid-state photochemical reactions for ten **CM** derivative crystals using the crystalline topochemical approach described in the Computational Methods section.[44] Consider first **4FCM**. While the HT and HH polymorph lattice energies differ by only 1.3 kJ/mol, the predicted solid-state photodimerization energies differ considerably. The reaction energy is endothermic by 55 kJ/mol in the HT crystal, but it increases to 80 kJ/mol in the HH crystal (Figure 9). Similar trends span the other eight solid-state photodimerization reactions examined. The average solid-state photodimerization energy for the HT crystals of **CM**, **4FCM**, **3ClCM**, **3CF$_3$CM**, and **24FCM** is 44 kJ/mol (range 40−55 kJ/mol). In contrast, the average computed solid-state reaction energy for the HH crystals of **3FCM**, **4FCM**, **25FCM**, **26FCM**, and **4CNCM** is 80% larger at 80 kJ/mol (range 69−100 kJ/mol). Similar endothermicity arguments were invoked previously to rationalize reactive and nonreactive anthracene crystals.[52]

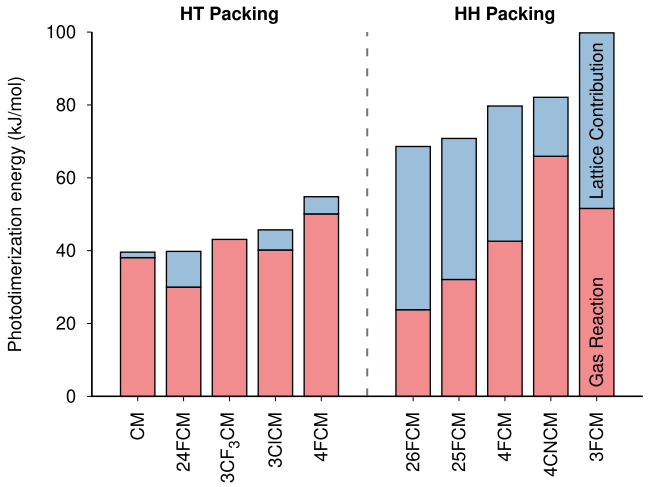

Figure 9. Predicted solid-state photodimerization energies, $E_{SSRD} - 2E_{monomer}$, for ten **CM** derivatives. The total reaction energies are partitioned into the gas-phase dimer reaction computed in the absence of the surrounding crystal lattice (using the crystalline dimer and SSRD geometries) in red, and the contributions from the surrounding lattice in blue.

To understand the origin of these reaction energy differences, we decompose the solid-state energy contributions for these 10 cases. Figure 9 separates the total solid-state reaction energy into the "gas-phase" contribution (obtained from gas-phase calculations on the reactant monomer pair and the product photodimer using geometries extracted directly from the DFT-optimized crystal structures) and the "lattice contribution" which indicates how the photodimerization energy changes in the presence of the surrounding lattice. For these ten systems, the average gas-phase reaction energies for HT (40 kJ/mol) and HH (43 kJ/mol) systems are very similar. Accounting for the rest of the crystal lattice contribution increases the HT reaction energies by only 4 kJ/mol on average but substantially increases the HH reaction energies by 37 kJ/mol on average.

Overall, the calculations thus far have revealed that HH crystal packing motifs are competitive with HT ones only when the HH monomer pairs can compensate by forming stronger interactions with the rest of the lattice. Because [2 + 2] photodimerization significantly deforms the molecular pair, the stronger interactions with HH lattices effectively inhibit the photodimerization of the monomer pairs.

4.3. Photomechanical Transformations in 3ClCM and 3CF$_3$CM. Finally, we investigate the experimental observation that the reactive HT polymorph of **3CF$_3$CM** exhibits stronger

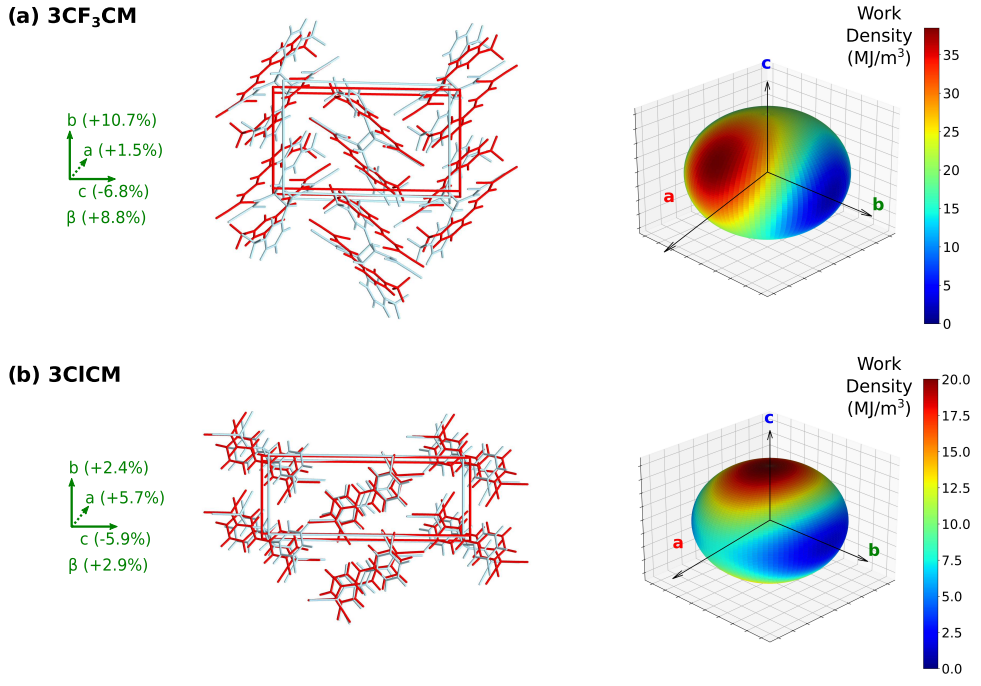

Figure 10. Predicted structural transformations resulting from the [2 + 2] photodimerization of the reactive polymorphs of (a) **3ClCM** and (b) **3CF$_3$CM**. The computed anisotropic photomechanical work densities (MJ/m^3) are also plotted. The larger change in lattice parameters for **3CF$_3$CM** results in a maximum work density that is almost twice as large as that for **3ClCM**.

https://doi.org/10.1021/acs.cgd.4c01033
Cryst. Growth Des. 2024, 24, 9544−9555

photosalience than the reactive polymorph of **3ClCM**, again using the topochemical approach to predict the photomechanical response properties. The modeling (Figure 10) indicates that both crystals exhibit small net volume changes upon photodimerization: **3ClCM** expands 1% and **3CF$_3$CM** contracts 0.3%. The buckling of the **3ClCM** molecules upon photodimerization elongates the *a* axis by 0.4 Å (5.7%) and increases the β angle by 2.9% (Figure 8). Photodimerization also effectively shortens the length of the molecule along its long axis, leading to a large 1.2 Å (5.9%) contraction along the *b* axis. Finally, a small 0.2 Å (2.4%) increase in the intermolecular spacing along the short **3ClCM** molecular axis occurs as well to reduce clashes between the adjacent photodimers. The photodimerization of **3CF$_3$CM** has a qualitatively similar behavior, though the molecular orientations relative to the unit cell axes differ. The molecular buckling from photodimerization expands the lattice 1.0 Å (10.7%) along the *b* axis. The lattice contracts 1.2 Å (6.8%) along the long molecular axis (*c* axis), and slightly expands 0.1 Å (1.5%) along the short molecular axis (*a* axis). Due to the herringbone nature of the packing, however, the lateral clashes created by CF_3 and other groups upon the photodimer buckling force the β angle to increase by a much larger 8.8%.

Given the significant anisotropy in the photomechanical structural response, it is unsurprising that the work density plots in Figure 10 are also highly anisotropic. While one might expect the expansion due to photodimer buckling to produce the most work density along the *b*-axis, the largest work density actually stems from the large *c* axis contraction in both crystals. That contraction occurs both because the photodimerized molecules become shorter along *c* due to the buckling and because the buckled photodimers exhibit more favorable C−H···Halogen interactions with nearby photodimers, especially for the larger CF_3 group. In **3CF$_3$CM**, the work density is further enhanced relative to **3ClCM** by the lateral steric clashes that induce the large β angle increase. Overall, the computed ∼40 MJ/m^3 work density of **3CF$_3$CM** is approximately double the ∼20 MJ/m^3 obtained for **3ClCM**, which could help explain the more violent photosalient response observed for **3CF$_3$CM**. Experimental verification of this work density would require measuring the force generated by a single crystal along a specific axis. The ability to perform such a measurement depends on obtaining the correct crystal habit, which is determined by both the crystal packing and the growth conditions. In this paper, we have not performed a systematic study of the crystal morphology but have identified a promising candidate (**3CF$_3$CM**) for optimization of growth conditions that would enable such force measurements.

5. CONCLUSIONS

In this paper, we have extended our previous results on the use of crystal engineering to create photomechanical crystals based on the **CM** motif. First, the synthesis of 12 new derivatives and experimental determination of their crystal structures has confirmed that the HT packing motif is required to observe the [2 + 2] photodimerization and photomechanical response. The reactivity differences between HH and HT crystals can be rationalized based on the generally stronger interactions HH monomer pairs form with their surrounding lattice, which in turn inhibits the molecular deformation associated with the [2 + 2] photodimerization. Because the formation of stronger interactions with the lattice appears to be a prerequisite for adopting HH packing, at least among these minimally modified **CM** species, we suspect that the reduced reactivity of HH-packed **CM** crystals is probably quite general. Second, based on these experimental results, we attempted to identify chemical substitution patterns that favor the reactive HT packing. Ideas based on simple steric and electrostatic considerations about how chemical substitution would affect HH versus HT packing were shown to be too naïve to have predictive value. Fluorination appears to generate both motifs in more-or-less random fashion. Computational results revealed that the competition between HH and HT is a complex, many-body interaction within the crystal lattice that cannot readily be explained by consideration of isolated monomer pairs. Nevertheless, we were able to identify an empirical trend in which substitution at the 3-position favors HT packing while substitution at the 4-position favors HH packing. Third, we wanted to get an idea of whether chemical substitution could affect the photomechanical work generation by an HT crystal. Preliminary results suggest that the answer is yes, with the molecule **3CF$_3$CM** generating a strong photosalient response experimentally, consistent with the 2× larger computed work density. Overall, our results suggest that the recipe for more powerful photomechanical crystals involves asymmetric substitution at the *meta* (3) position in order to increase molecular size while maintaining HT packing and photoreactivity. The **CM** system provides a useful case study to illustrate how molecular structure, crystal packing, and polymorphism must all be considered when designing a functional molecular crystal.

■ ASSOCIATED CONTENT

Supporting Information

The Supporting Information is available free of charge at https://pubs.acs.org/doi/10.1021/acs.cgd.4c01033.

Images of the crystal packing; synthesis procedures for the compounds; NMR spectra of compounds and select intermediate compounds; crystal structure data and collection procedures; optical absorption spectra; additional calculation results and energy decomposition plots (PDF)

Six videos are available showing molecular motion or the photosalient effect of the crystals when exposed to light; Video S1: **3CF$_3$CM** exhibiting a photosalient effect (MP4)

Video S2: **3ClCM** exhibiting a photosalient effect (MP4)

Video S3: **3BrCM** exhibiting a photosalient effect (MP4)

Video S4: **4BrCM** not exhibiting a photosalient effect (MP4)

Video S5: **4ClCM** not exhibiting a photosalient effect (MP4)

Video S6: **3CF$_3$CM** in glycerol showing motion (MP4)

Accession Codes

Deposition Numbers 2371403−2371416 contain the supplementary crystallographic data for this paper. These data can be obtained free of charge via the joint Cambridge Crystallographic Data Centre (CCDC) and Fachinformationszentrum Karlsruhe Access Structures service.

https://doi.org/10.1021/acs.cgd.4c01033
Cryst. Growth Des. 2024, 24, 9544−9555

AUTHOR INFORMATION

Corresponding Authors

Gregory J. O. Beran − *Department of Chemistry, University of California, Riverside, Riverside, California 92521, United States;* orcid.org/0000-0002-2229-2580; Email: gregory.beran@ucr.edu

Rabih O. Al-Kaysi − *College of Science and Health Professions-3124, King Saud bin Abdulaziz University for Health Sciences, and King Abdullah International Medical Research Center (Nanomedicine), Ministry of National Guard Health Affairs, Riyadh 11426, Kingdom of Saudi Arabia;* orcid.org/0000-0001-8429-2802; Email: rabihalkaysi@gmail.com

Christopher J. Bardeen − *Department of Chemistry, University of California, Riverside, Riverside, California 92521, United States; Materials Science and Engineering, University of California, Riverside, Riverside, California 92521, United States;* orcid.org/0000-0002-5755-9476; Email: christopher.bardeen@ucr.edu

Authors

Thomas J. Gately − *Department of Chemistry, University of California, Riverside, Riverside, California 92521, United States;* orcid.org/0000-0001-6199-4764

Cody J. Perry − *Department of Chemistry, University of California, Riverside, Riverside, California 92521, United States*

Sophie Weiss − *Materials Science and Engineering, University of California, Riverside, Riverside, California 92521, United States*

Kevin Lam − *Department of Chemistry, University of California, Riverside, Riverside, California 92521, United States;* orcid.org/0009-0007-6606-8170

Imadul Islam − *College of Science and Health Professions-3124, King Saud bin Abdulaziz University for Health Sciences, and King Abdullah International Medical Research Center (Nanomedicine), Ministry of National Guard Health Affairs, Riyadh 11426, Kingdom of Saudi Arabia*

Mohammed N. Almtiri − *College of Science and Health Professions-3124, King Saud bin Abdulaziz University for Health Sciences, and King Abdullah International Medical Research Center (Nanomedicine), Ministry of National Guard Health Affairs, Riyadh 11426, Kingdom of Saudi Arabia;* orcid.org/0000-0002-4108-0604

Veronica Carta − *Department of Chemistry, University of California, Riverside, Riverside, California 92521, United States;* orcid.org/0000-0001-8089-8436

Complete contact information is available at: https://pubs.acs.org/10.1021/acs.cgd.4c01033

Notes

The authors declare no competing financial interest.

ACKNOWLEDGMENTS

This work was supported by the National Science Foundation, grant DMR-1810514 to C.J.B., and CHE-1955554 to G.J.O.B. R.O.K. acknowledges support from the King Abdullah International Medical Research Center (KSAU-HS/KAIMRC) through Grant NRC21R25003. Computer time to G.J.O.B. from ACCESS (CHE110064) and the UC Riverside High-Performance Computing Center, which was funded by the NSF (MRI-2215705, MRI-1429826) and NIH (1S10OD016290-01A1), is also gratefully acknowledged.

REFERENCES

(1) Desiraju, G. R. *Crystal Engineering: The Design of Organic Solids*; Elsevier, 1989.

(2) Nangia, A. K.; Desiraju, G. R. Crystal Engineering: An Outlook for the Future. *Angew. Chem., Int. Ed.* **2019**, *58*, 4100−4107.

(3) Cohen, M. D.; Schmidt, G. M. J.; Sonntag, F. I. 384. Topochemistry. Part II. The Photochemistry of trans-Cinnamic Acids. *J. Chem. Soc.* **1964**, 2000−2013.

(4) Schmidt, G. M. J. 385. Topochemistry. Part III. The Crystal Chemistry of Some trans-Cinnamic Acids. *J. Chem. Soc.* **1964**, 2014−2021.

(5) Schmidt, G. M. J. Photodimerization in the Solid State. *Pure Appl. Chem.* **1971**, *27* (4), 647−678.

(6) Friscic, T.; MacGillivray, L. R. Single-Crystal-to-Single-Crystal [2 + 2] Photodimerizations: from Discovery to Design. *Z. Kristallogr. - Cryst. Mater.* **2005**, *220*, 351−363.

(7) MacGillivray, L. R.; Papaefstathiou, G. S.; Friscic, T.; Hamilton, T. D.; Bucar, D. K.; Chu, Q.; Varshney, D. B.; Georgiev, I. G. Supramolecular control of reactivity in the solid state: from templates to ladderanes to metal-organic frameworks. *Acc. Chem. Res.* **2008**, *41*, 280−291.

(8) Hema, K.; Ravi, A.; Raju, C.; Pathan, J. R.; Rai, R.; Sureshan, K. M. Topochemical polymerizations for the solid-state synthesis of organic polymers. *Chem. Soc. Rev.* **2021**, *50*, 4062−4099.

(9) Naumov, P.; Kowalik, J.; Solntsev, K. M.; Baldridge, A.; Moon, J.-S.; Kranz, C.; Tolbert, L. M. Topochemistry and photomechanical effects in crystals of green fluorescent protein-like chromophores: effects of hydrogen bonding and crystal packing. *J. Am. Chem. Soc.* **2010**, *132*, 5845−5857.

(10) Kim, T.; Zhu, L.; Mueller, L. J.; Bardeen, C. J. Dependence of the solid-state photomechanical response of 4-chlorocinnamic acid on crystal shape and size. *CrystEngComm* **2012**, *14*, 7792−7799.

(11) Wang, H.; Chen, P.; Wu, Z.; Zhao, J.; Sun, J.; Lu, R. Bending, Curling, Rolling, and Salient Behavior of Molecular Crystals Driven by [2 + 2] Cycloaddition of a Styrylbenzoxazole Derivative. *Angew. Chem., Int. Ed.* **2017**, *56*, 9463−9467.

(12) Peng, J.; Ye, K.; Liu, C.; Sun, J.; Lu, R. The photomechanic effects of the molecular crystals based on 5-chloro-2-(naphthalenylvinyl)benzoxazols fueled by topo-photochemical reactions. *J. Mater. Chem. C* **2019**, *7*, 5433−5441.

(13) Liu, J.; Ye, K.; Shen, Y.; Peng, J.; Sun, J.; Lu, R. Photoactuators based on the dynamic molecular crystals of naphthalene acrylic acids driven by stereospecific [2 + 2] cycloaddition reactions. *J. Mater. Chem. C* **2020**, *8*, 3165−3175.

(14) Shu, Y.; Ye, K.; Yue, Y.; Sun, J.; Wang, H.; Zhong, J.; Yang, X.; Gao, H.; Lu, R. Fluorine as a robust balancer for tuning the reactivity of topo-photoreactions of chalcones and the photomechanical effects of molecular crystals. *CrystEngComm* **2021**, *23*, 5856−5868.

(15) Chen, Y.-R.; Jia, M.-Z.; Pan, J.-Q.; Tan, B.; Zhang, J. Photomechanical behavior triggered by [2 + 2] cycloaddition and photochromism of a pyridinium-functionalized coordination complex. *Dalton Trans.* **2022**, *51*, 6157−6161.

(16) Xu, T.-Y.; Tong, F.; Xu, H.; Wang, M.-Q.; Tian, H.; Qu, D.-H. Engineering Photomechanical Molecular Crystals to Achieve Extraordinary Expansion Based on Solid-State [2 + 2] Photocycloaddition. *J. Am. Chem. Soc.* **2022**, *144*, 6278−6290.

(17) Wang, L.; Qiao, S.-B.; Chen, Y.-T.; Ma, X.; Wei, W.-M.; Zhang, J.; Du, L.; Zhao, Q.-H. [2 + 2] cycloaddition and its photomechanical effects on 1D coordination polymers with reversible amide bonds and coordination site regulation. *Chem. Sci.* **2024**, *15*, 3971−3979.

(18) Medishetty, R.; Husain, A.; Bai, Z.; Runceviski, T.; Dinnebier, R. E.; Naumov, P.; Vittal, J. J. Single crystals popping under UV light: a photosalient effect triggered by a [2 + 2] cycloaddition reaction. *Angew. Chem., Int. Ed.* **2014**, *53*, 5907−5911.

(19) Kole, G. K.; Kojima, T.; Kawano, M.; Vittal, J. J. Reversible Single-Crystal-to-Single-Crystal Photochemical Formation and Ther-

mal Cleavage of a Cyclobutane Ring. *Angew. Chem., Int. Ed.* **2014**, *53*, 2143−2146.
(20) Medishetty, R.; Sahoo, S. C.; Mulijanto, C. E.; Naumov, P.; Vittal, J. J. Photosalient Behavior of Photoreactive Crystals. *Chem. Mater.* **2015**, *27*, 1821−1829.
(21) Yadava, K.; Vittal, J. J. Photosalient Behavior of Photoreactive Zn(II) Complexes. *Cryst. Growth Des.* **2019**, *19*, 2542−2547.
(22) Rath, B. B.; Vittal, J. J. Single-Crystal-to-Single-Crystal [2 + 2] Photocycloaddition Reaction in a Photosalient One-Dimensional Coordination Polymer of Pb(II). *J. Am. Chem. Soc.* **2020**, *142*, 20117−20123.
(23) Rath, B. B.; Vittal, J. J. Photoreactive Crystals Exhibiting [2 + 2] Photocycloaddition Reaction and Dynamic Effects. *Acc. Chem. Res.* **2022**, *55*, 1445−1455.
(24) Naumov, P.; Sahoo, S. C.; Zakharov, B. A.; Boldyreva, E. V. Dynamic Single Crystals: Kinematic Analysis of Photoinduced Crystal Jumping (The Photosalient Effect). *Angew. Chem., Int. Ed.* **2013**, *52*, 9990−9995.
(25) McGehee, K.; Saito, K.; Kwaria, D.; Minamikawa, H.; Norikane, Y. Releasing a bound molecular spring with light: a visible light-triggered photosalient effect tied to polymorphism. *Phys. Chem. Chem. Phys.* **2024**, *26*, 6834−6843.
(26) Tong, F.; Xu, W.; Guo, T.; Lui, B. F.; Hayward, R. C.; Palffy-Muhoray, P.; Al-Kaysi, R. O.; Bardeen, C. J. Photomechanical molecular crystals and nanowire assemblies based on the [2 + 2] photodimerization of a phenylbutadiene derivative. *J. Mater. Chem. C* **2020**, *8*, 5036−5044.
(27) Row, T. N. G.; Swamy, H. R.; Acharyaa, K. R.; Ramamurthy, V.; Venkatesan, K.; Rao, C. N. R. Reversible Photodimerization of Phenylbutadienes in the Solid State. *Tetrahedron Lett.* **1983**, 3263−3266.
(28) Gately, T. J.; Cook, C.; Almuzarie, R.; Islam, I.; Gardner, Z.; Iuliucci, R. J.; Al-Kaysi, R. O.; Beran, G. J. O.; Bardeen, C. J. Effect of Fluorination on the Polymorphism and Photomechanical Properties of Cinnamalmalononitrile Crystals. *Cryst. Growth. Des.* **2022**, *22*, 7298−7307.
(29) Szalewicz, K. Symmetry-adapted perturbation theory of intermolecular forces. *Wiley Interdiscip. Rev.: Comput. Mol. Sci.* **2012**, *2*, 254−272.
(30) Hohenstein, E. G.; Sherrill, C. D. Density fitting of intramonomer correlation effects in symmetry-adapted perturbation theory. *J. Chem. Phys.* **2010**, *133*, No. 014101.
(31) Smith, D. G. A.; Burns, L. A.; Simmonett, A. C.; Parrish, R. M.; Schieber, M. C.; Galvelis, R.; Kraus, P.; Kruse, H.; Di Remigio, R.; Alenaizan, A.; et al. Psi4 1.4: Open-source software for high-throughput quantum chemistry. *J. Chem. Phys.* **2020**, *152* (18), No. 184108.
(32) Papajak, E.; Truhlar, D. G. What are the most efficient basis set strategies for correlated wave function calculations of reaction energies and barrier heights? *J. Chem. Phys.* **2012**, *137*, No. 064110.
(33) Parker, T. M.; Burns, L. A.; Parrish, R. M.; Ryno, A. G.; Sherrill, C. D. Levels of symmetry adapted perturbation theory (SAPT). I. Efficiency and performance for interaction energies. *J. Chem. Phys.* **2014**, *140*, No. 094106.
(34) Giannozzi, P.; Andreussi, O.; Brumme, T.; Bunau, O.; Nardelli, M. B.; Calandra, M.; Car, R.; Cavazzoni, C.; Ceresoli, D.; Cococcioni, M.; et al. Advanced capabilities for materials modelling with Quantum ESPRESSO. *J. Phys.: Condens. Matter* **2017**, *29*, No. 465901.
(35) Becke, A. D. On the large-gradient behavior of the density functional exchange energy. *J. Chem. Phys.* **1986**, *85*, 7184−7187.
(36) Perdew, J. P.; Burke, K.; Ernzerhof, M. Generalized Gradient Approximation Made Simple. *Phys. Rev. Lett.* **1996**, *77*, 3865−3868.
(37) Otero-de-la-Roza, A.; Johnson, E. R. Van der Waals interactions in solids using the exchange-hole dipole moment model. *J. Chem. Phys.* **2012**, *136*, No. 174109.
(38) Bryenton, K. R.; Adeleke, A. A.; Dale, S. G.; Johnson, E. R. Delocalization error: The greatest outstanding challenge in density-functional theory. *Wiley Interdiscip. Rev.: Comput. Mol. Sci.* **2023**, *13*, No. e1631.
(39) Beran, G. J. O.; Greenwell, C.; Cook, C.; Řezáč, J. Improved Description of Intra- and Intermolecular Interactions through Dispersion-Corrected Second-Order Møller−Plesset Perturbation Theory. *Acc. Chem. Res.* **2023**, *56*, 3525−3534.
(40) Beran, G. J. O. Solid state photodimerization of 9-tert-butyl anthracene ester produces an exceptionally metastable polymorph according to firstprinciples calculations. *CrystEngComm* **2019**, *21*, 758−764.
(41) Greenwell, C.; Beran, G. J. O. Inaccurate Conformational Energies Still Hinder Crystal Structure Prediction in Flexible Organic Molecules. *Cryst. Growth Des.* **2020**, *20*, 4875−4881.
(42) Santra, G.; Sylvetsky, N.; Martin, J. M. L. Minimally Empirical Double-Hybrid Functionals Trained against the GMTKN55 Database: revDSD-PBEP86-D4, revDOD-PBE-D4, and DOD-SCAN-D4. *J. Phys. Chem. A* **2019**, *123*, 5129−5143.
(43) Neese, F. The ORCA program system. *Wiley Interdiscip. Rev.: Comput. Mol. Sci.* **2012**, *2*, 73−78.
(44) Cook, C. J.; Li, W.; Lui, B. F.; Gately, T. J.; Al-Kaysi, R. O.; Mueller, L. J.; Bardeen, C. J.; Beran, G. J. O. A theoretical framework for the design of molecular crystal engines. *Chem. Sci.* **2023**, *14*, 937−949.
(45) Cook, C. J.; Perry, C. J.; Beran, G. J. O. Organic Crystal Packing Is Key to Determining the Photomechanical Response. *J. Phys. Chem. Lett.* **2023**, *14*, 6823−6831.
(46) Uscumlic, G. S.; Krstic, V. V.; Muskatirovic, M. D. Correlation of Ultraviolet Absorption Frequences of Cis and Trans Substituted Cinnamic Acids with Hammett Substituent Constants. *J. Mol. Struct.* **1988**, *174*, 251−254.
(47) Barker, C. C.; Bride, M. H.; Hallas, G.; Stamp, A. 249. Steric Effects in Di- and Tri-arylmethanes. Part III. Electronic Absorption Spectra of Derivatives of Malachite Green containing Substituents in the Phenyl Ring. *J. Chem. Soc.* **1961**, 1285−1290.
(48) Dürüst, Y.; Yildirim, M. Synthesis, UV−Vis spectra, and Hammett correlation of some novel bis(dihydropyrrolo[3,4-c]-pyrazoles). *Monatsh. Chem.* **2010**, *141*, 961−973.
(49) van Beek, L. K. H. A relationship between dipole moments and the Hammett equation. *Recl. Travaux Chem. Pays-Bas* **1957**, *76*, 729−732.
(50) Rao, C. N. R.; Wahl, W. H.; Williams, E. J. A Correlation of Electric Dipole Moments of Substituted Benzenes by Reactivities. *Can. J. Chem.* **1957**, *35*, 1575−1578.
(51) Ramamurthy, V.; Venkatesan, K. Photochemical reactions of organic crystals. *Chem. Rev.* **1987**, *87*, 433−481.
(52) Gately, T. J.; Sontising, W.; Easley, C. J.; Islam, I.; Al-Kaysi, R. O.; Beran, G. J. O.; Bardeen, C. J. Effect of halogen substitution on energies and dynamics of reversible photomechanical crystals based on 9-anthracenecarboxylic acid. *CrystEngComm* **2021**, *23*, 5931−5943.

https://doi.org/10.1021/acs.cgd.4c01033
Cryst. Growth Des. 2024, 24, 9544−9555